to zero via spin-lattice relaxation. The initial buildup rates of the NOE's depend only on the cross relaxation coefficients between the irradiated spin and the observed nuclei, and are thus directly related to the inverse of the sixth power of the proton-proton distances in the three-dimensional structure of the protein.

The following are some details to be observed in the transient NOE's of Figures 2 and 3. At $\tau = 0$, the line corresponding to the geminal methylene proton with respect to the pulsed nucleus has already emerged because of spin diffusion during the 15 ms of the pulse duration. In Figure 3 the additional appearance of the methyl signal ϵ in the $\tau = 0$ trace is a trivial consequence of the limited selectivity of the inversion pulse applied to the line γ'. In both Figures 2 and 3 a line at 3.1 ppm grows at about the same rate as the β-methylene signals of Met 80. From two decoupled NOE difference spectra, where, respectively, the β or β' line was irradiated for spin pumping prior to spin decoupling during data acquisition,[7,8] this resonance was independently assigned to the α proton of Met 80. It is seen that the α-proton resonance grows faster when the γ' peak is pulsed than when the γ peak is pulsed. In Figure 3 the α-proton resonance has already appeared at $\tau = 25$ ms, whereas it has not emerged until 50 ms in Figure 2.

Corresponding transient NOE's were obtained after application of selective inversion pulses to the resonances β and β' (Figure 1). It was found that the α-proton line of Met 80 grows faster after irradiation of resonance β' than after irradiation of β. In an additional experiment the resonances γ and γ' were found to grow faster than β and β' after pulse inversion of the Met 80 methyl line ϵ.

From these experiments the increased information content of transient NOE studies in macromolecules (Figures 2 and 3) as compared to the more conventional steady-state experiments (Figure 1) is readily apparent. While the steady-state NOE was able to distinguish between the β- and γ-methylene protons, the transient NOE's further distinguished between β and β' and γ and γ', respectively, of the axial Met 80. These assignments agree with those generally accepted,[14] which were originally suggested from ring-current calculations based on the X-ray structure.[13] The transient NOE's provided further information on static and dynamic aspects of the spatial arrangement of Met 80 in the protein. The different growth rates of the α-proton line (Figures 2 and 3) clearly show that the protons β' and γ' are located more closely to the α proton than the protons β and γ. Since they are at higher field (Figure 1), the β' and γ' protons must also be closest to the heme ring plane. That the different local environments of the individual β- and γ-methylene protons are manifested in the transient NOE's further shows that the rotational mobility about the single bonds in the side chain of Met 80 is severely limited in ferrocytochrome *c*. Finally, experiments of the type of Figures 2 and 3 provide a convincing demonstration of spin diffusion pathways in proteins. Overall, the present experiments imply that spin diffusion in macromolecules, rather than leading necessarily to less specific and hence less useful NOE's,[2,9] may through suitable use of the two-dimensional frequency-time space of transient NOE experiments lead to novel insights into the molecular structures which might not be available otherwise.

Acknowledgments. Financial support by the Roche Research Foundation for Scientific Exchange and Biomedical Collaboration with Switzerland (fellowship to S. L. Gordon) and the Swiss National Science Foundation (project 3.0046.76) is gratefully acknowledged.

References and Notes

(1) Noggle, J. H.; Schirmer, R. E. "The Nuclear Overhauser Effect", Academic Press: New York, 1971.
(2) Kalk, A.; Berendsen, H. J. C. *J. Magn. Reson.* **1976**, *24*, 343–366.
(3) Balaram, P.; Bothner-By, A. A.; Dadok, J. *J. Am. Chem. Soc.* **1972**, *94*, 4015–4017.
(4) Campbell, I. D.; Dobson, C. M.; Williams, R. J. P. *J. Chem. Soc., Chem. Commun.* **1974**, 888–889.
(5) Glickson, J. D.; Gordon, S. L.; Pittner, T. P.; Agresti, D. G.; Walter, R. *Biochemistry.* **1976**, *15*, 5721–5729.
(6) Keller, R. M.; Wüthrich, K. *Biochim. Biophys. Acta.* **1978**, *533*, 195–208.
(7) Richarz, R.; Wüthrich, K. *J. Magn. Reson.* **1978**, *30*, 147–150.
(8) Wüthrich, K.; Wagner, G.; Richarz, R.; Perkins, S. J. *Biochemistry.* **1978**, *17*, 2253–2263.
(9) Hull, W. E.; Sykes, B. D. *J. Chem. Phys.* **1975**, 867–880.
(10) Solomon, I. *Phys. Rev.* **1955**, *99*, 559–565.
(11) Experiments of the type discussed in this communication were alluded to in the closing paragraph of ref 2. Transient NOE experiments on small molecules have been carried out frequently, for example, Freeman, R.; Hill, H. D. W.; Tomlinson, B. L. *J. Chem. Phys.* **1974**, *61*, 4466–4473.
(12) Wüthrich, K. *Proc. Natl. Acad. Sci. U.S.A.* **1969**, *63*, 1071–1078.
(13) McDonald, C. C.; Phillips, W. D. *Biochemistry.* **1973**, *12*, 3170–3186.
(14) Cookson, D. J.; Moore, G. R.; Pitt, R. C.; Williams, R. J. P.; Campbell, I. D.; Ambler, R. P.; Bruschi, M.; Le Gall, J. *Eur. J. Biochem.* **1978**, *83*, 261–275.
(15) Sodium 2,2,3,3-tetradeuterio-3-trimethylsilylpropionate.
(16) Free induction decays.
(17) School of Chemistry, Georgia Institute of Technology, Atlanta, Georgia 30332.

Sidney L. Gordon,*[17] Kurt Wüthrich*
Institut für Molekularbiologie und Biophysik
Eidgenössische Technische Hochschule
CH-8093 Zürich-Hönggerberg, Switzerland
Received May 17, 1978

Analogues of Metallic Lattices in Rhodium Carbonyl Cluster Chemistry. Synthesis and X-ray Structure of the $[Rh_{15}(\mu\text{-}CO)_{14}(CO)_{13}]^{3-}$ and $[Rh_{14}(\mu\text{-}CO)_{16}(CO)_9]^{4-}$ Anions Showing a Stepwise Hexagonal Close-Packed/Body-Centered Cubic Interconversion

Sir:

We have already reported the isolation and characterization of two members of a family of rhodium carbonyl cluster anions, $[Rh_{13}(CO)_{24}H_{5-n}]^{n-}$ ($n = 2, 3$), containing a metal atom polyhedron which is part of a hexagonal close-packed lattice.[1] These have been studied by X-ray diffraction[1,2] and by NMR spectroscopy.[3] We report here the characterization of two new high nuclearity rhodium clusters which show different types of metal atom packings. The structural relationships between these two new clusters and the above Rh_{13} species are also discussed.

The mild pyrolysis of $Na_2[Rh_{12}(CO)_{30}]$ or of mixtures of $Rh_4(CO)_{12}$ and NaOH (2.5–3 OH^- for every 15 Rh atoms) in 2-propanol under nitrogen at 80 °C for 10–20 h gives a mixture of brown anionic species. Separation is achieved by fractional precipitation of the alkali metal salts from aqueous solution: after precipitation of sodium salts, potassium salts can be obtained from which $K_3(diglyme)_x[Rh_{15}(CO)_{27}]$ can be separated (15–20% yield) because of its insolubility in diglyme. Metathesis with Me_4N^+ and Et_4N^+ chlorides in methanol gives the corresponding crystalline salts; the ^1H NMR spectrum of the Et_4N^+ salt shows the absence of metal hydrides.

The Me_4N^+ salt has been investigated by X-ray diffraction[4] and the metallic skeleton of the $[Rh_{15}(CO)_{27}]^{3-}$ anion is illustrated schematically in Figure 1a, while Figure 1b shows the metallic coordination around the central metal atom. The metal atom cluster may formally be derived from the polyhedron of D_{3h} symmetry, which contains that part of the hexagonal close-packed array found in the $[Rh_{13}(CO)_{24}H_{5-n}]^{n-}$ ($n = 2, 3$) cluster (Figure 2), by capping two square faces ((2, 3, 6, 7) and (9, 11, 13, 14) in Figure 1a). However, while the bottom part of the polyhedron follows this hexagonal close

0002-7863/78/1500-7096$01.00/0

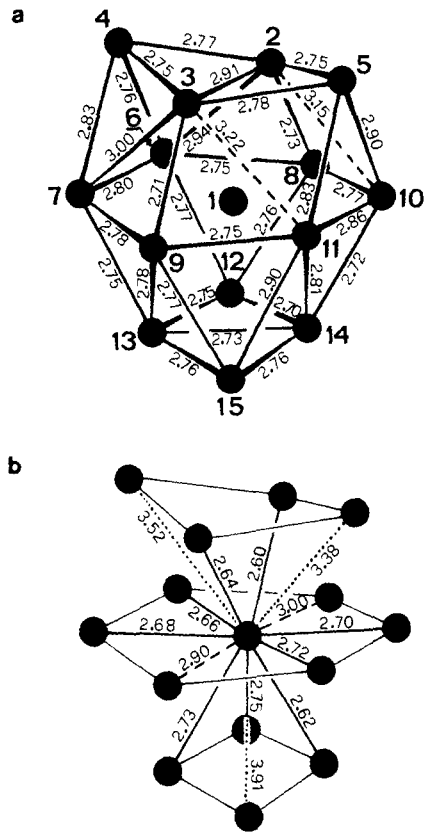

Figure 1. The metal atom cluster in the $[Rh_{15}(CO)_{27}]^{3-}$ anion with the surface metal-metal bonds (a) and the center to surface ones (b). Mean standard deviation 0.005 Å.

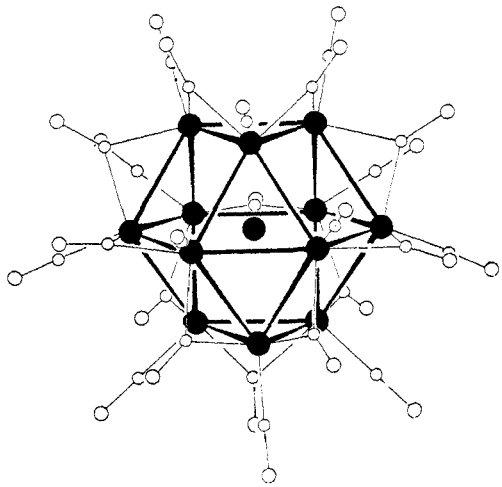

Figure 2. A view of the $[Rh_{13}(CO)_{24}H_{5-n}]^{n-}$ (n = 2, 3) anions.

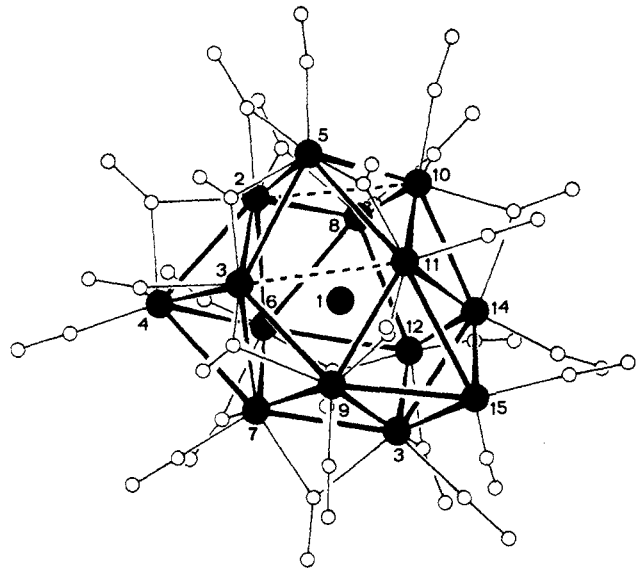

Figure 3. A view of the anion $[Rh_{15}(CO)_{27}]^{3-}$ showing the carbonyls' stereochemistry.

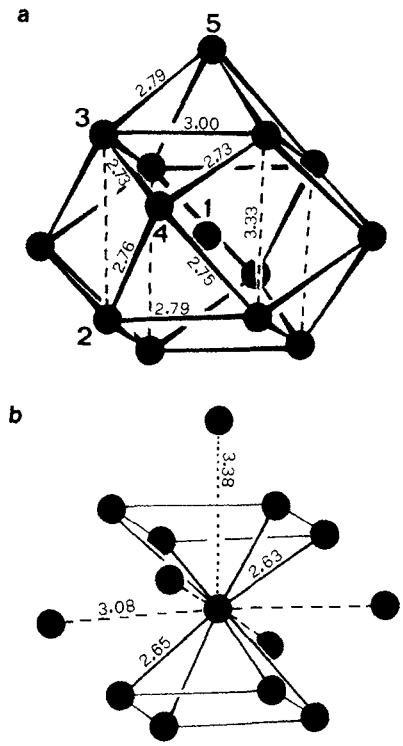

Figure 4. The metal atom cluster in the $[Rh_{14}(CO)_{25}]^{4-}$ anion with the surface metal-metal bonds (a) and the center to surface ones (b). Mean standard deviation 0.005 Å.

packing, as confirmed by the 6 + 3 coordination shown by the central metal atom in this half of the cluster, the upper part is considerably distorted because atoms 2 and 3 have moved over the central metal with concomitant lengthening of the 2-6 and 3-7 distances and shortening of the 2-10 and 3-11 distances (broken lines). In this part of the cluster the atoms 2, 3, 6, 7, 10, and 11 define one half of a cube which contains metal atom 1 at the center. The essentially body-centered cubic arrangement present in this half of the cluster is confirmed by the 4 + 2 coordination of the central metal atom shown in Figure 1b. Actually two of the six bonds in the hexagonal plane, involving atoms 8 and 9, are longer than the other four, the lengthening being ascribed to the hcp → bcc interconversion.

The metal-metal distances found for $[Rh_{15}(CO)_{27}]^{3-}$ are rather scattered: there are 36 normal contacts ranging from 2.60 to 2.86 Å (average 2.74 Å), 7 intermediate contacts from 2.90 to 3.00 Å (average 2.94 Å), and 5 long interactions from 3.15 to 3.91 Å.

The complete anion is illustrated in Figure 3. There are 13 terminal and 14 edge-bridging CO groups; all of the skeletal metal atoms except 15, are bonded to three carbonyls. The 13 terminal groups are irregularly distributed: 2 are on metal atom 15 whereas none are on atoms 2 and 3, and the remaining rhodium atoms each contain one terminal carbonyl. The mean values for the Rh-C and C-O bond lengths for terminal and bridging CO are 1.83, 1.17 Å and 2.00, 1.19 Å, respectively.

In acetonitrile, fragmentation of $[Rh_{15}(CO)_{27}]^{3-}$ occurs on reaction with bromide to give the $[Rh(CO)_2Br_2]^-$ and $[Rh_{14}(CO)_{25}]^{4-}$ anions:

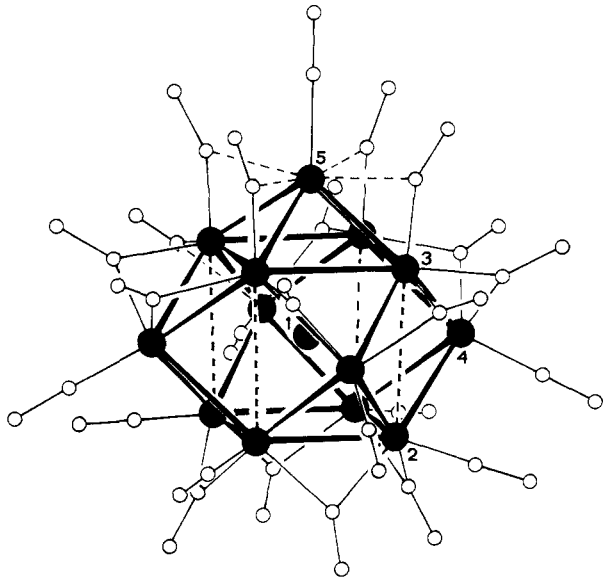

Figure 5. A view of the $[Rh_{14}(CO)_{25}]^{4-}$ anion. A fourfold crystallographic axis passes through atoms 1 and 5.

$$[Rh_{15}(CO)_{27}]^{3-} + 2Br^- \xrightarrow{MeCN} [Rh_{14}(CO)_{25}]^{4-} + [Rh(CO)_2Br_2]^-$$

ν_{CO} 2040 (vw), 1998 (s, Br), 1850-1825-1805 (m, br) cm^{-1}	ν_{CO} 1960 (s), 1930 (sh, br), 1805 (m) cm^{-1}

This new tetraanion has been isolated as the crystalline Et_4N^+ salt in nearly quantitative yield. IR spectra suggest that addition of $[Rh(CO)_2(MeCN)_2]BF_4$ to an acetonitrile solution of $[Rh_{14}(CO)_{25}]^{4-}$ results in quantitative conversion of the tetranion to the starting $[Rh_{15}(CO)_{27}]^{3-}$ trianion.

The metallic skeleton of the $[Rh_{14}(CO)_{25}]^{4-}$ tetraanion is illustrated in Figure 4a, while Figure 4b shows the coordination around the central metal atom. The metallic polyhedron corresponds to an incomplete rhombic dodecahedron elongated along the crystallographic quaternary axis passing through atoms 1 and 5. Figure 4b clearly shows that this structure is essentially part of a body-centered cubic lattice. Of the independent metal-metal interactions 8 are normal bonds ranging from 2.63 to 2.79 Å (average 2.73 Å), 2 are intermediate (3.00 and 3.08 Å) and 2 are long (3.33 and 3.38 Å) contacts.

The complete anion is illustrated in Figure 5. There are 9 terminal and 16 edge-bridging CO groups, and all of the skeletal metal atoms, except 5, are bonded to 3 carbonyls; the low coordination of atom 5 is apparently compensated by the formation of 4 strongly asymmetric CO bridges (Rh(5)-C = 2.30 (4) Å, Rh(3)-C = 1.75 (4) Å). The mean values for the Rh-C and C-O bond lengths for the terminal and symmetric edge-bridging carbonyls are 1.77, 1.19 Å and 2.00, 1.18 Å, respectively. Comparison of Figures 3 and 5 shows that the metal atom which is removed on passing from the Rh_{15} to the Rh_{14} anion seems to be that labeled 15 in Figure 3, i.e., the metal which has two terminal CO groups. The disposition of the carbonyl groups in the remaining part of the Rh_{15} anion strictly resembles that in the Rh_{14} cluster and is similar to that previously observed in the $[Rh_{13}(CO)_{24}H_{5-n}]^{n-}$ (n = 2, 3) anions.

Comparison of the structures observed for the Rh_{13} and Rh_{14} clusters is analogous to the transformation between hcp and bcc lattices which is well known for many metals.[6] Comparison of the structures of Rh_{13} or Rh_{14} with the Rh_{15} structure is analogous to surface reconstruction, which is again well known for a number of metals.[7] Both analogies are in agreement with the belief that large clusters are real models of small metallic crystallites covered (or poisoned) by ligands.

Further work is in progress on these families of clusters.

Acknowledgment. We thank the Italian C.N.R. for financial support.

References and Notes

(1) V. G. Albano, A. Ceriotti, P. Chini, G. Ciani, S. Martinengo, and W. M. Anker, *J. Chem. Soc. Chem. Commun.*, 859 (1975).
(2) V. G. Albano, G. Ciani, S. Martinengo, and A. Sironi, *J. Chem. Soc., Dalton, Trans.*, in press.
(3) S. Martinengo, B. T. Heaton, R. J. Goodfellow, and P. Chini, *J. Chem. Soc., Chem. Commun.*, 39 (1977).
(4) The salt $[Me_4N]_3[Rh_{15}(CO)_{27}]$ crystallizes in the monoclinic space group $P2_1/n$ (No. 14) with cell constants a = 12.658 (4) Å, b = 22.485 (9) Å, c = 22.848 (8) Å, β = 91.52 (3)°, Z = 4. The structure has been solved by direct methods and refined by least squares using 3730 independent significant counter data. The refinements are in progress, the current R value being 8.3%.
(5) The salt $[Et_4N]_4[Rh_{14}(CO)_{25}]$ crystallizes in the tetragonal space group $P4/ncc$ (No. 130) with cell constants a = 17.056 (2) Å, c = 27.186 (4) Å, Z = 4. The structure has been solved by Patterson and Fourier methods on the basis of 876 independent significant counterdata. The refinements are in progress, the current R value being 5.2%.
(6) A. F. Wells, "Structural Inorganic Chemistry", Oxford University Press, London, 1975, p 1015.
(7) G. A. Somorjai and L. L. Kesmodel, "International Review of Science, Physical Chemistry Series Two", Vol. 7, M. Kerker, Ed., Butterworths, London, p 15.

Secondo Martinengo*
Centro del C.N.R. sui bassi stati di ossidazione
Via G. Venezian 21, 20133—Milan, Italy

Gianfranco Ciani, Angelo Sironi, Paolo Chini
Istituto di Chimica Generale dell'Università
Via G. Venezian 21, 20133—Milan, Italy

Received May 17, 1978

Diel-Alder Cycloaddition of Juglone Derivatives: Elucidation of Factors Influencing Regiochemical Control

Sir:

In connection with studies directed toward tetracycline total synthesis, Inhoffen and Muxfeldt reported an interesting observation: the nature of the oxygen function in 5-hydroxy- (**1**) and 5-acetoxy-1,4-naphthoquinone (**2**) profoundly influenced the regiochemistry of the cycloaddition with 1-acetoxybutadiene.[1] This general trend has been noted subsequently for a variety of diene systems by several groups, notably Birch,[2] Kelly,[3] and Trost.[4a]

The rationale for this effect, alluded to initially by Inhoffen and further developed by Birch[2] and Kelly,[3] revolves around the concept that the strong hydrogen bond known to be present in quinone **1** serves as an "internal Lewis acid" polarizing the unsaturated system and resulting in the C-4 carbonyl serving as the dominant director of cycloaddition. Alternatively, electron donation by the oxygen is considered to dominate in the acetate **2** (and methyl ether **6**) leading to reversal of the regiochemical result.

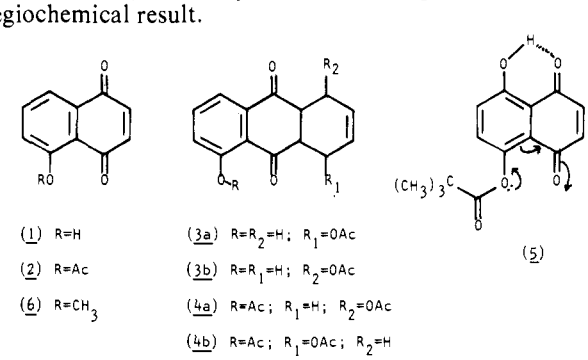

(1) R=H
(2) R=Ac
(6) R=CH_3

(3a) R=R_2=H; R_1=OAc
(3b) R=R_1=H; R_2=OAc
(4a) R=Ac; R_1=H; R_2=OAc
(4b) R=Ac; R_1=OAc; R_2=H

(5)

0002-7863/78/1500-7098$01.00/0